

**MICROSTRUCTURES AND RHEOLOGY OF  
A LIMESTONE-SHALE THRUST FAULT**

A Thesis

by

RACHEL KRISTEN WELLS

Submitted to the Office of Graduate Studies of  
Texas A&M University  
in partial fulfillment of the requirements for the degree of

MASTER OF SCIENCE

December 2010

Major Subject: Geology

**MICROSTRUCTURES AND RHEOLOGY OF  
A LIMESTONE-SHALE THRUST FAULT**

A Thesis

by

RACHEL KRISTEN WELLS

Submitted to the Office of Graduate Studies of  
Texas A&M University  
in partial fulfillment of the requirements for the degree of

MASTER OF SCIENCE

Approved by:

Chair of Committee,	Julie Newman
Committee Members,	Will Lamb
	Adam Klaus
Head of Department,	Andreas Kronenberg

December 2010

Major Subject: Geology

## ABSTRACT

Microstructures and Rheology of a Limestone-Shale Thrust Fault.

(December 2010)

Rachel Kristen Wells, B.S., The University of Texas at Austin

Chair of Advisory Committee: Dr. Julie Newman

The Copper Creek thrust fault in the southern Appalachians places Cambrian over Ordovician sedimentary strata. The fault accommodated displacement of 15-20 km at 100-180 °C. Along the hanging wall-footwall contact, microstructures within a ~2 cm thick calcite and shale shear zone suggest that calcite, not shale, controlled the rheology of the shear zone rocks. While shale deformed brittlely, plasticity-induced fracturing in calcite resulted in ultrafine-grained (<1.0  $\mu\text{m}$ ) fault rocks that deformed by grain boundary sliding (GBS) accommodated primarily by diffusion creep, suggesting low flow stresses.

Optical and electron microscopy of samples from a transect across the footwall shale into the shear zone, shows the evolution of rheology within the shear zone. Sedimentary laminations 1 cm below the shear zone are cut by minor faults, stylolites, and fault-parallel and perpendicular calcite veins. At vein intersections, calcite grain size is reduced (to ~0.3  $\mu\text{m}$ ), and microstructures include inter-and-intragranular fractures, four-grain junctions, and interpenetrating boundaries. Porosity rises to 6% from <1% in coarse (25  $\mu\text{m}$ ) areas of calcite veins. In coarse-grained calcite, trails of

voids follow twin boundaries, and voids occur at twin-twin and twin-grain boundary intersections.

At the shear zone-footwall contact, a 350  $\mu\text{m}$  thick calcite band contains coarse- and ultrafine-grained layers. Ultrafine-grained ( $\sim 0.34 \mu\text{m}$ ) layers contain microstructures similar to those at vein intersections in the footwall and display no lattice-preferred orientation (LPO). Coarse-grained layers cross-cut grain-boundary alignments in the ultrafine-grained layers; coarse grains display twins and a strong LPO. Within the shear zone, ultrafine-grained calcite-aggregate clasts and shale clasts (5-350  $\mu\text{m}$ ) lie within an ultrafine-grained calcite ( $< 0.31 \mu\text{m}$ ) and shale matrix. Ultrafine-grained calcite ( $< 0.31 \mu\text{m}$ ) forms an interconnected network around the matrix shale.

Calcite vein microstructures suggest veins continued to form during deformation. Fractures at twin-twin and twin-grain boundary intersections suggest grain size reduction by plasticity-induced fracturing, resulting in  $< 1 \mu\text{m}$  grains. Interpenetrating boundaries, four-grain junctions, and no LPO indicate the ultrafine-grained calcite deformed by viscous grain boundary sliding. The evolution of the ultrafine-grain shear zone rocks by a combination of plastic and brittle processes and the deformation of the interconnected network of ultrafine-grained calcite by viscous GBS enabled a large displacement along a narrow fault zone.

## ACKNOWLEDGEMENTS

I would like to thank my committee chair, Dr. Julie Newman, and my committee members, Dr. Will Lamb and Dr. Adam Klaus, for their guidance and support throughout the course of this research. I want to give an extended thanks to Dr. Steven Wojtal for his guidance in the development of, and throughout, the research. This research was supported by American Association of Petroleum Geologist Halbouty Grant, Sigma Xi, and Texas A&M Graduate Enhancement Fund. The FE-SEM acquisition was supported by the National Science Foundation grant DBI-0116835, the Vice President for Research Office, and the Texas Engineering Experimental Station.

I would like to thank Kristen Mullen, Caleb Holyoke, Ray Guillemette, Tom Stephens, Harold Johnson, and Mike Tice for assistance. Thanks also go to my friends and colleagues and the department faculty and staff for making my time at Texas A&M University a great experience.

Finally, thanks to my parents and sister for their continued encouragement.

**NOMENCLATURE**

BSE	Backscatter electrons
CL	Cathodoluminescence
CC	Copper Creek thrust
EBSD	Electron backscatter diffraction
EDS	Energy dispersive spectroscopy
FW	Footwall
GBS	Grain boundary sliding
HW	Hanging wall
LPO	Lattice preferred orientation
SEM	Scanning electron microscopy
SZ	Shear zone
TEM	Transmission electron microscopy
SE	Secondary electrons
WDS	Wavelength dispersive spectroscopy

## TABLE OF CONTENTS

	Page
ABSTRACT .....	iii
ACKNOWLEDGEMENTS .....	v
NOMENCLATURE.....	vi
TABLE OF CONTENTS .....	vii
LIST OF FIGURES.....	viii
1. INTRODUCTION.....	1
2. GEOLOGIC SETTING.....	4
3. METHODS.....	6
4. RESULTS.....	7
4.1 Shale layer .....	9
4.2 Densely-veined shale.....	13
4.3 Calcite band.....	14
4.4 Shear zone.....	18
5. DISCUSSION.....	20
5.1 Grain size reduction .....	20
5.2 Multiple deformation mechanism .....	21
5.2.1 Calcite.....	21
5.2.2 Shale .....	24
5.3 Mixing of ultrafine-grained calcite and shale within shear zone.....	24
5.4 Intermittent vein formation.....	25
5.5 Evolution of fault zone rheology.....	26
6. CONCLUSIONS .....	30
REFERENCES .....	32
VITA .....	36

**LIST OF FIGURES**

	Page
Figure 1 Structure map of the CC thrust fault .....	5
Figure 2 Exposure of the CC thrust fault.....	8
Figure 3 Sample at FW-SZ contact .....	8
Figure 4 Calcite veins and void orientations .....	10
Figure 5 Calcite grain size and long axis orientations.....	11
Figure 6 Cross-cut calcite veins in shale .....	12
Figure 7 Calcite microstructures.....	15
Figure 8 EBSD data.....	17
Figure 9 Shear zone microstructures .....	19



## 1. INTRODUCTION

The ability of large thrust sheets to move long distances along narrow zones has been a subject of great debate in efforts to understand the formation of fold-and-thrust belts. In early work to resolve this problem, Hubbert and Rubey (1959) proposed that increased fluid pressure along a thrust fault may reduce normal stress, allowing thrust sheets to move large distances along a narrow zone. Later, Dahlen et al. (1984), Dahlen (1990), and Davis and Engelder (1985) proposed that internal deformation within the thrust sheet accommodates deformation until a critical taper is reached, at which point the sheet easily slides along a weak layer - a localized zone of deformation. Much work has focused on the rheology and evolution of the rocks within these localized zones of deformation (e.g., Mitra, 1984; Wojtal and Mitra, 1986; O'Hara, 1988; 1990, Newman and Mitra, 1993;1994; Kennedy and Logan, 1997;1998; Liu et al., 2002). Along foreland thrusts, one common observation is the presence of shale along major thrust faults, which has been thought to act as a weak layer allowing large displacements (e.g., Wiltschko and Chapple, 1977; Thomas, 2001; Ikari et al, 2009). Shale may contribute to the weakness of a fault zone by increasing the fluid pressure and reducing friction (e.g., Cobbold et al., 2009).

The Copper Creek (CC) thrust fault, in the southern Appalachians, is a classic example of a foreland thrust fault that exhibits a narrow shear zone (~2 cm) that accommodated large displacement (~15 km) (e.g., Suppe, 1985; Wojtal and Mitra, 1986). As observed along other foreland thrusts, this fault contains shale layers

---

This thesis follows the style of Journal of Structural Geology.

in both hanging wall and footwall along much of the length of the fault as well as numerous calcite veins. Recent work on the CC thrust, as well as other foreland thrusts such as the Hunter Valley in the southern Appalachians and the McConnell thrust in the Canadian Rockies, has suggested that fluids played an important role in deformation, but due to its role in enhancing diffusive mass transfer (e.g., Wojtal and Mitra, 1986) and/or dislocation creep (Kennedy and Logan, 1997; 1998) rather than by increasing fluid pressure. These previous studies, using optical microscopy as well as observations from transmission electron microscopy (TEM), document evidence for multiple deformation mechanisms, including fracturing, diffusive mass transfer, and crystal plasticity.

However, due to limitations on the resolution of the optical microscope, and limits on the area observed using TEM, interactions between deformation mechanisms, and the relative contributions of different deformation mechanisms, are difficult to discern.

Using a high-resolution scanning electron microscope (FEI Quanta 600 FE-SEM), this study documents microstructures at a scale that allows observation of spatial relations between microstructures in a transect across the narrow shear zone, thus addressing 1) the relative contributions of shale and calcite to the deformation and 2) the role of different deformation mechanisms, and their interactions, on the evolution of the weak, narrow zone.

Consistent with results from previous work on foreland thrusts in general, and the CC thrust in particular, I conclude that fluids played a critical role in deformation and localization along the fault. Calcite veins were emplaced parallel to the shear zone, suggesting high fluid pressures in the vicinity of the fault. While the emplacement of

these veins may have provided some contribution to displacement along the fault, their critical contribution was in providing starting material for the fault zone rocks.

Deformation along the fault was dominated by ultrafine grained ( $<1.0 \mu\text{m}$ ) calcite that had been emplaced as coarser-grained veins. This contribution focuses on the deformation of these carbonate veins and the footwall shale along the narrow transition (2 cm) from non-penetratively deformed footwall shale to the shear zone.

## 2. GEOLOGIC SETTING

The Copper Creek thrust, eastern Tennessee, is one of approximately 20 foreland thrusts located in the transition from the Blue Ridge to the Valley and Ridge of the southern Appalachian fold-and-thrust belt (Harris, 1976; Harris and Milici, 1977; Wojtal, 1986; Wojtal and Mitra, 1986) (Figure 1). Reconstructed cross-sections across the region estimate that the fault accommodated offset of 15-20 km with an overburden of 4-6 km (Harris, 1976; Harris and Milici, 1977; Wojtal and Mitra, 1986), suggesting temperatures of 100-180 °C (assuming 30°C/km) during deformation. The hanging wall along the CC thrust is Cambrian shale with interbedded limestone and the footwall consists of Ordovician carbonates with interbedded shale (Wojtal, 1986; Lemiszki and Kohl, 2006).

The Copper Creek thrust exposure, north of Knoxville, TN, is bound by shale in both the HW and FW at the studied location. The HW/FW contact contains a ~2 cm thick band of intensely deformed rocks, oriented N20°W. Mesoscale structures in the hanging wall and footwall consist of numerous minor faults, fractures, folds, stylolites, and cross-cutting veins (Wojtal, 1986; Wojtal and Mitra, 1986).

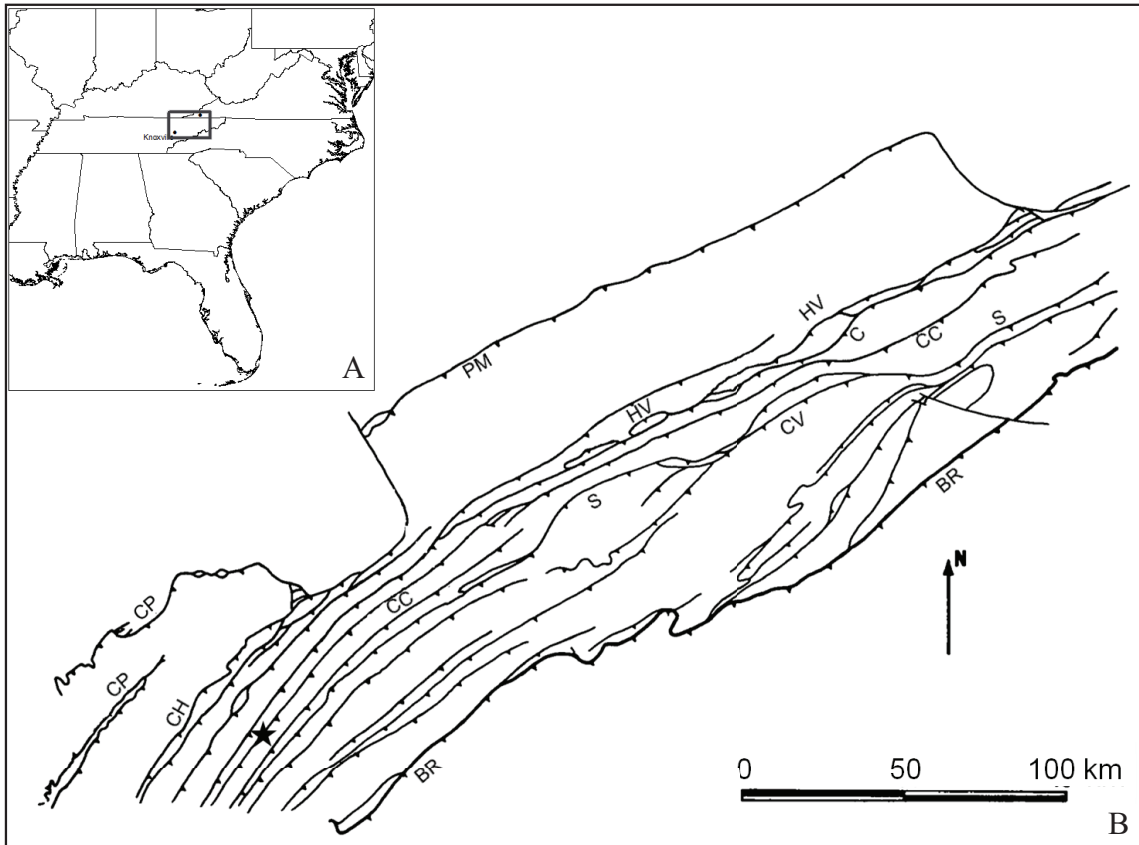


**Figure 1.** Structure map of the CC thrust fault. (A) Location of thrust faults in eastern Tennessee, near Knoxville. (B) Generalized structure map (after Wojtal, 1986). CC-Copper Creek thrust, HV-Hunter Valley thrust, CP-Cumberland Plateau, BR-Blue Ridge, S-Saltville thrust, CV-Carter Valley thrust, CH-Chattanooga thrust, PM-Pine Mountain thrust, C-Clinchport thrust. Location of exposure of CC thrust used in this study (star).

### 3. METHODS

Samples for microstructural investigation were collected along a transect from 3 m above the hanging wall to 4 m below the shear zone in the footwall (Figure 2). Standard and ultrathin sections were made from the collected samples, oriented perpendicular to the shear zone foliation, and parallel to the shear zone lineation. Optical microscopy was used to select samples for detailed study. Because of the fine-grained nature of these rocks, much of the observation was carried out using secondary (SE) and backscattered electron (BSE) imaging on the scanning electron microscope (SEM: FEI Quanta 600 FE-SEM housed in the Microscopy and Imaging Center, Texas A&M University). Electron backscatter diffraction (EBSD: Channel 5, Oxford Instruments) on the SEM was used to determine the lattice-preferred orientations (LPO) of calcite grains. Grain size, void size, and shape preferred orientations were determined by image analysis (Image SXM) on figures made by tracing grains on overlays on BSE images. The number, thickness, and orientation of veins were measured in linear transects oriented  $\pm 45^\circ$  from the shear zone foliation. Porosity was determined using ImageSXM on thresholded BSE images of polished samples. Compositional analyses were carried out using x-ray fluorescence (XRF), wavelength dispersive spectroscopy (WDS), and energy dispersive spectroscopy (EDS). Cathodoluminescence (CL) images were obtained using both optical and electron microscopy.

#### 4. RESULTS

The Copper Creek thrust contains a 2 cm thick, light gray layer at the hanging wall-footwall contact with a 30 cm-thick coherent shale bed in its footwall and a 6 cm thick shale bed in its hanging wall (Figure 2). Very little penetrative deformation is observed in the hanging wall or footwall beyond the shear zone. This study focuses on the transition from the footwall into the shear zone (Figure 3). At 1 cm below the shear zone-footwall contact, sedimentary laminations are observed in the shale, cross-cut by veins of calcite and calcite + ankeritic dolomite. Stylolites also occur within the footwall, perpendicular to the shear zone, with spacings of 50-300  $\mu\text{m}$ .

Within the footwall shale, the calcite is confined to veins, while within the shear zone it is intermixed with shale. The contact between the shear zone and the footwall is marked by a 300  $\mu\text{m}$  thick continuous calcite layer composed of multiple calcite veins. The 2 cm transition from non-penetrative deformation within the footwall shale to the shear zone is seen clearly and can be divided into four layers based on microstructural (Figure 3a) and compositional (Figure 3b) variations.

The layer farthest from the footwall-shear zone contact ( $> 1$  cm below the contact) is a *non-penetratively deformed shale layer*. In this layer, deformation of calcite veins is observed where fault-parallel veins cross-cut and displace fault-perpendicular veins. Above the *shale layer* is the *densely-veined shale layer*, which contains shale and more calcite veins than the layer below. The 300  $\mu\text{m}$  thick *calcite band* forms the contact between the *densely-veined shale* and the *shear zone*. The *shear zone* is



**Figure 2.** Exposure of the CC thrust fault. Copper Creek thrust fault 32 km north of Knoxville, TN. The footwall (FW) is composed of shale and micrite beds, while the hanging wall (HW) is composed of shale, carbonate, and sandstone beds. The hanging wall is displaced to the north. Samples taken near the FW-HW contact (circles).

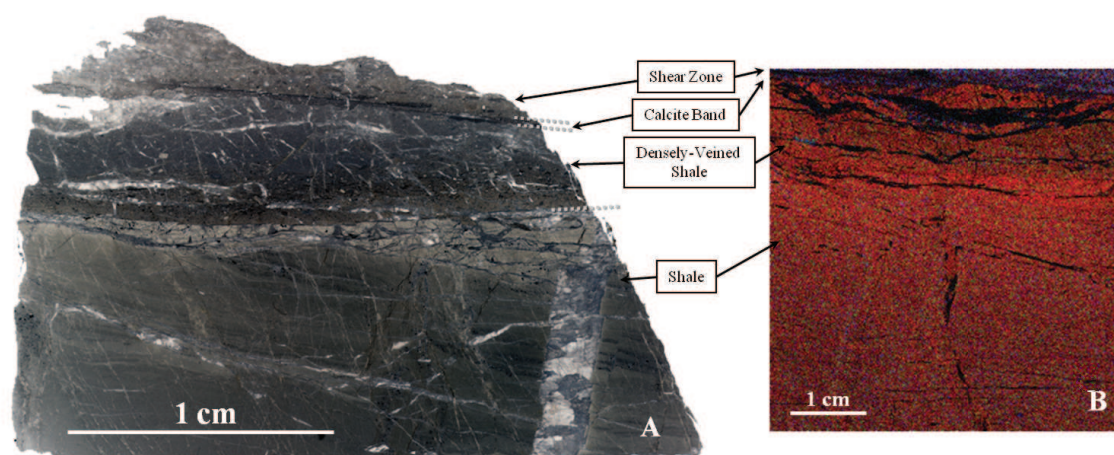


**Figure 3.** Sample at FW-SZ contact. (A) Sample across footwall-shear zone contacts. Sample is divided into four distinct layers based on composition and microstructures: *shale layer*, *densely-veined shale*, *calcite band*, and *shear zone*. (B) Calcite veins (black) are oriented parallel or perpendicular to the shear foliation. Shear zone contains Ca, Al, and K. XRF image. Si-red, Al-green, K-blue, Ca-black.



composed of foliated bands of calcite, shale and intermixed calcite and shale.

Deformation within the footwall is observed predominantly within calcite veins. CL, at the optical and electron microscope scale, indicates no variation in luminescence of calcite across the transition from the footwall shale to the shear zone. The microstructures within each layer are described below.

#### *4.1 Shale layer*

The footwall host rock shale is composed of illite with chlorite, quartz, and calcite. The shale contains sedimentary laminations that are cross-cut by calcite veins (0.88 fractures/mm; mean thickness 289.3  $\mu\text{m}$ ) approximately parallel and perpendicular to the shear zone, although most (66 %) are orientated at a low angle to the shear zone (Figure 4a). There is a discontinuous layer of silica-rich shale at the top of the *shale layer*, which is fractured and contains carbonate veins. Calcite grains in undeformed sections of the veins have a mean grain size of 73.41  $\mu\text{m}$  (Figure 5a), with an average axial ratio of 1:1.8. The long axes are variably oriented, with a weak maximum at a low angle ( $\sim 20^\circ$ ) to the shear zone (Figure 5a).

Deformation within the calcite veins is observed where veins approximately parallel to the shear zone cross-cut and displace veins approximately perpendicular to the shear zone (Figure 3a; 6a). Within these vein intersections, grain size is reduced to  $<1.0 \mu\text{m}$  (average grain size 0.87  $\mu\text{m}$ ; Figure 5b). These ultrafine grains contain

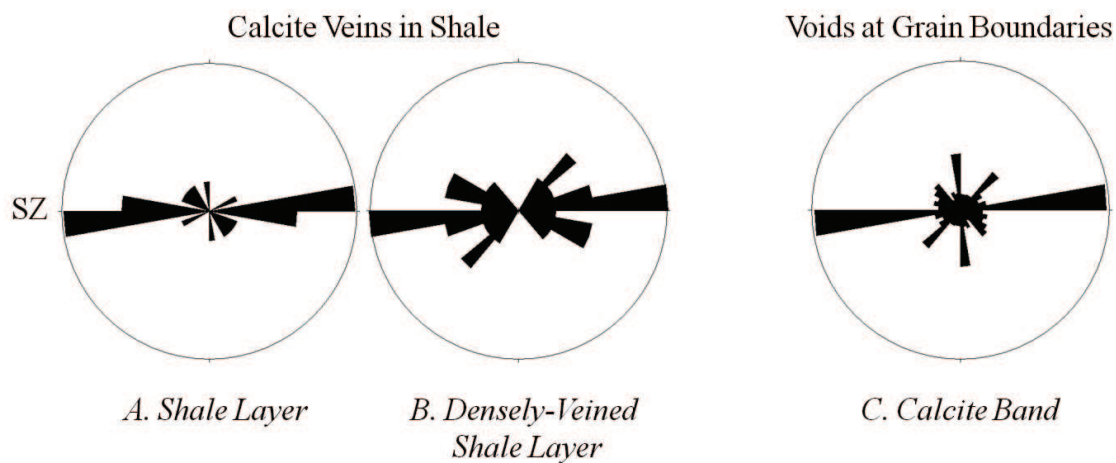


**Figure 4.** Calcite veins and void orientations. (A) Calcite veins in *shale layer* and (B) *densely-veined shale layers* plotted relative to orientation of shear zone (SZ). (C) Voids plotted relative to orientation of shear zone.

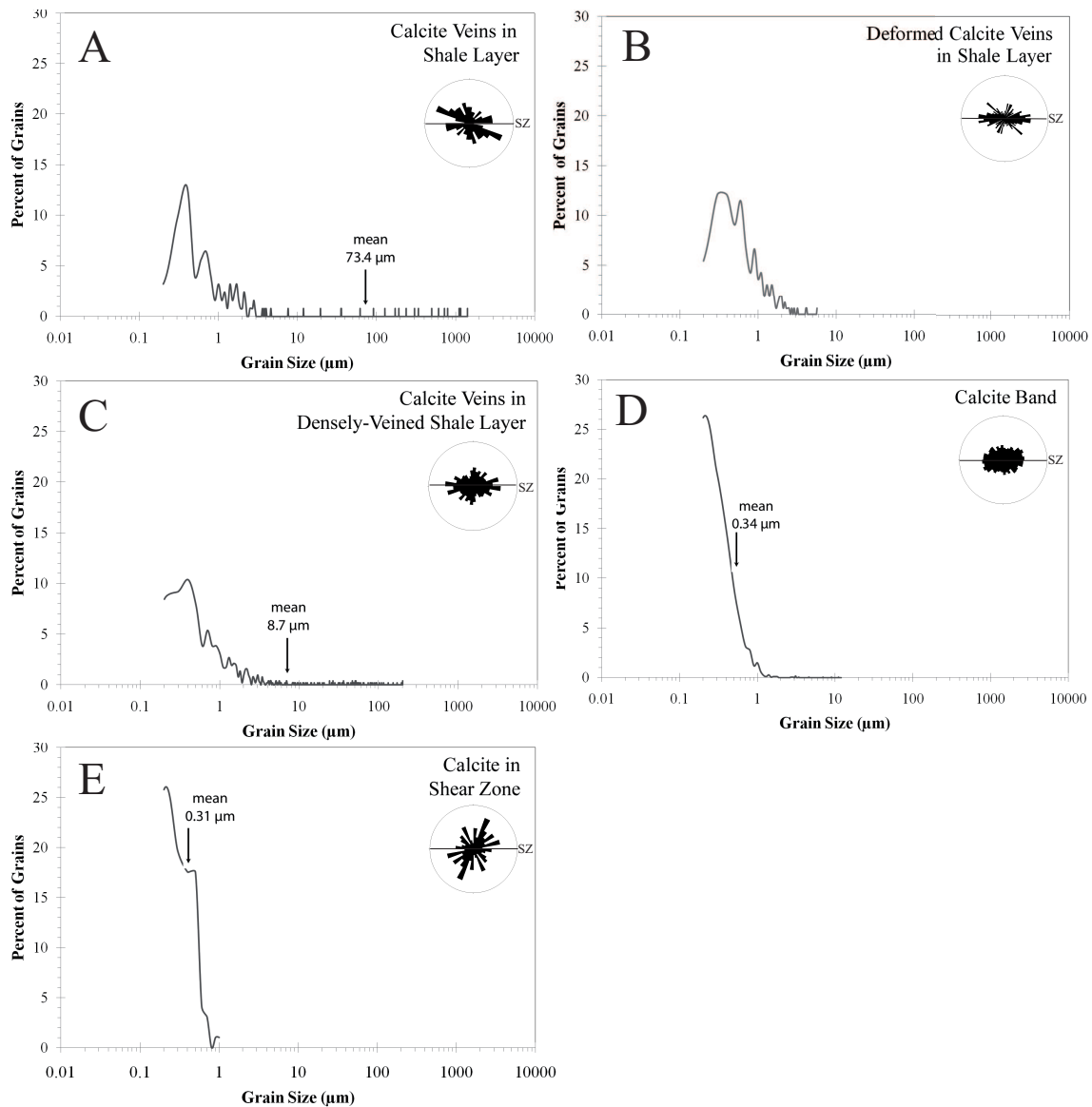


**Figure 5.** Calcite grain size and long axis orientations. Calcite grain size vs. the percent of total calcite grains. The mean grain size and range of grain sizes within a layer decreases towards the shear zone. Insets show long-axes of calcite grains in the veins in footwall-shear zone layers plotted relative to the orientation of the shear zone (SZ).

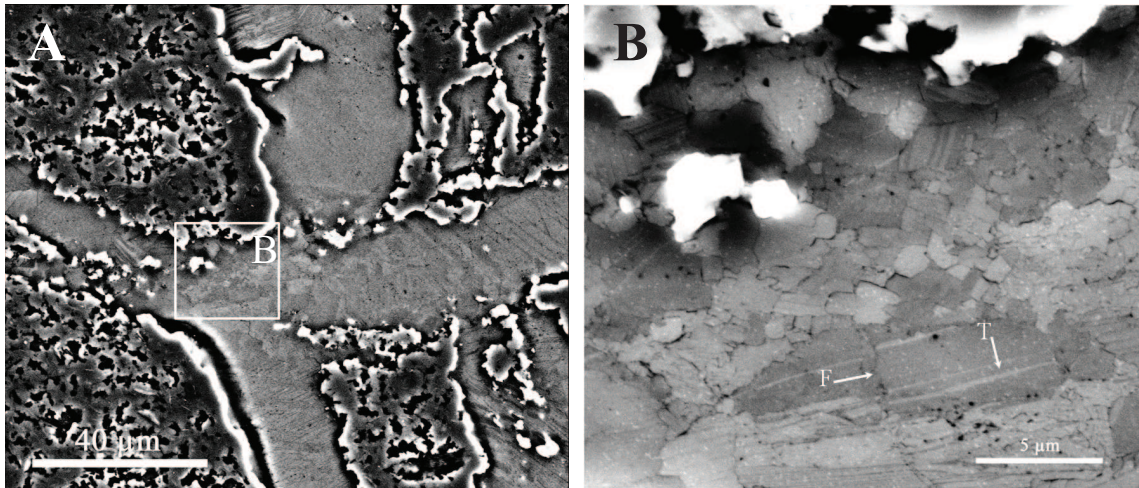


**Figure 6.** Cross-cut calcite veins in shale. (A) Cross-cut calcite veins in *shale layer*. (B) Ultrafine-grained calcite at intersection of cross-cut veins contain fractures ("F" arrow), twins ("T" arrow), and interpenetrating grain boundaries. BSE imaging.

twins, and fractures, and voids are common at calcite grain boundaries (Figure 6b). Long axes of calcite grains within vein intersections are dominantly oriented parallel to the displacement of the cross-cut vein (Figure 5b). Voids have a mean size of  $0.26\ \mu\text{m}$ , with long axes also dominantly oriented parallel to the displacement of the cross-cut vein.

#### 4.2 *Densely-veined shale*

Within the *densely-veined shale*, sedimentary laminations are observed only locally. The shale in this layer has a higher density of veins (1.46 fractures/mm; mean thickness is  $146.9\ \mu\text{m}$ ) relative to the *shale layer* below (Figure 3a). The orientations of the veins in this layer are also more variable than in the layer below, although many veins (45 %) are still at a low angle to the shear zone (Figure 4b). The mean grain size within the calcite veins is  $8.69\ \mu\text{m}$  in coarse-grained areas of veins (Figure 5c). Calcite grains have an average axial ratio of 1:2.2 with long axes variable, but dominantly at a low angle to the shear zone (Figure 5c).

Within this layer, a higher percentage of the calcite veins (~80%) contain fine to ultrafine grains ( $<5\ \mu\text{m}$ ) than the veined shale described in section 4.1. Twins are visible primarily within the coarser calcite grains (Figure 7a). In coarse-grains, trails of voids are common (Figure 7a). The trails follow twin boundaries in grains, and voids are observed at twin-twin and twin-grain boundary intersections (Figure 7b). Locally, irregular twin boundaries are also observed within coarser calcite grains (Figure 7b). In

regions of fine-grained calcite, inter- and intragranular fractures, interpenetrating grain boundaries, twins, and voids along calcite grain boundaries are common (Figure 7c, 4c).

#### 4.3 Calcite band

Between the *densely-veined shale* and the *shear zone* is a band of calcite (~ 300  $\mu\text{m}$  total thickness) intermixed with minor shale (less than 6 % shale). The mean calcite grain size within this band alternates between layers with grain size  $\leq 1 \mu\text{m}$ , and coarser-grained layers with grain size 1 – 30  $\mu\text{m}$  (Figure 5d). Calcite grains within the coarser-grained (mean grain size of 5.5  $\mu\text{m}$ ) calcite layers have an axial ratio of 1:1.4 and straight grain boundaries. Voids and shale particles are only very rarely observed within the coarser calcite layers (porosity less than 1 %). The dominant microstructure observed within the coarse calcite layers is twinning (Figure 7d).

Coarse- and ultrafine-grained layers are occasionally separated by narrow areas with an intermediate grain size (mean grain size is 2  $\mu\text{m}$ ), containing voids and minor shale (1-2% each). Grain boundaries of the intermediate grains are often curved (Figure 7d) and variations in grayscale within individual grains are observed in the BSE images of these single phase areas (Figure 7d).

The mean grain size within the ultrafine-grained layer is 0.34  $\mu\text{m}$  (Figure 5d), with a long axis-preferred orientation parallel to the shear zone (axial ratio of 1:1.9) (Figure 5d). Porosity and shale within the ultrafine-grain layers increases to ~6 % and 4.5%, respectively. The average void diameter is 0.07  $\mu\text{m}$ , with an axial ratio of 1:2. Most long axes of the voids are 10° anticlockwise from the shear zone foliation

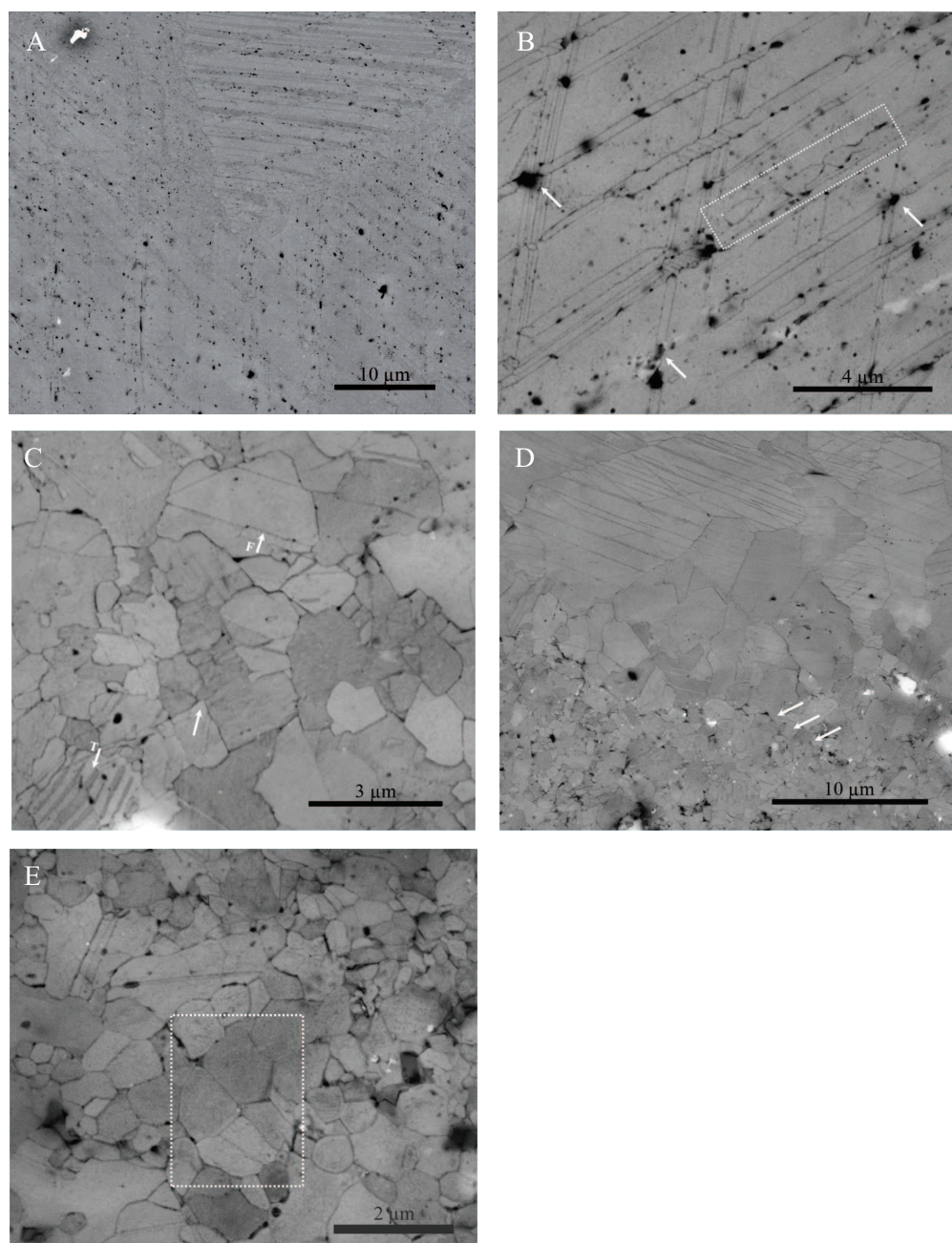


**Figure 7.** Calcite microstructures. (A) Trails of voids (black) follow twin boundaries. *Densely-veined shale layer.* (B) Voids at twin-twin intersections (arrow). Irregular twin boundaries are rare (dashed area). *Densely-veined shale layer.* (C) Intragranular fractures ("F" arrow), twins ("T" arrow), interpenetrating grain boundaries, and grid pattern in ultrafine-grained calcite (arrow). *Densely-veined shale layer.* (D) Boundary between coarse-grained calcite and ultrafine-grained calcite layers. Aligned grain boundaries (arrows) in ultrafine-grained calcite cross-cut by coarse-grained calcite. *Calcite band.* (E) Four-grain junction (dashed area). *Calcite band.* BSE imaging.



(Figure 4c). Long-axis orientations of the voids are parallel to the vein orientations in shale layers below (Figure 4). Microstructures within the ultrafine-grain layers include twins, intragranular fractures, interpenetrating grain boundaries (most common), voids at grain boundaries, and four-grain junctions (Figure 7f). Twins are observed rarely within the ultrafine-grains, and where observed, are frequently cross-cut by fractures. A majority of the ultrafine-grained calcite grains contain angular to rounded interpenetrating grain boundaries, which are not cross-cut by fractures. The grains that form four-point junctions also contain interpenetrating grain boundaries between each other and adjacent grains. Linear features defined by aligned grain boundaries across several grains (minimum length 4  $\mu\text{m}$ ) are developed within the calcite band, at a low angle ( $\sim 23^\circ$ ) to the shear zone (Figure 7d, Figure 8a). The coarser-grained calcite layers, which are parallel to the shear zone, cross-cut these linear features (Figure 7d, Figure 8a).

The lattice preferred orientations of calcite grains were determined along a transect from a coarser-grained ( $> 5 \mu\text{m}$ ) calcite layer into an ultrafine-grained ( $< 1 \mu\text{m}$ ) calcite layer (Figure 8a, 8b). Orientations of grains from a coarse calcite layer indicate a strong LPO, with c-axes oriented perpendicular to the shear zone foliation (Figure 8c). In contrast, orientations of grains from the adjacent ultrafine-grained layer suggest no LPO (Figure 8d). In addition, the orientation map of the ultrafine-grained layer (Figure 8b) shows no similarities in orientations between adjacent grains (i.e., no groupings of grains of a given orientation).



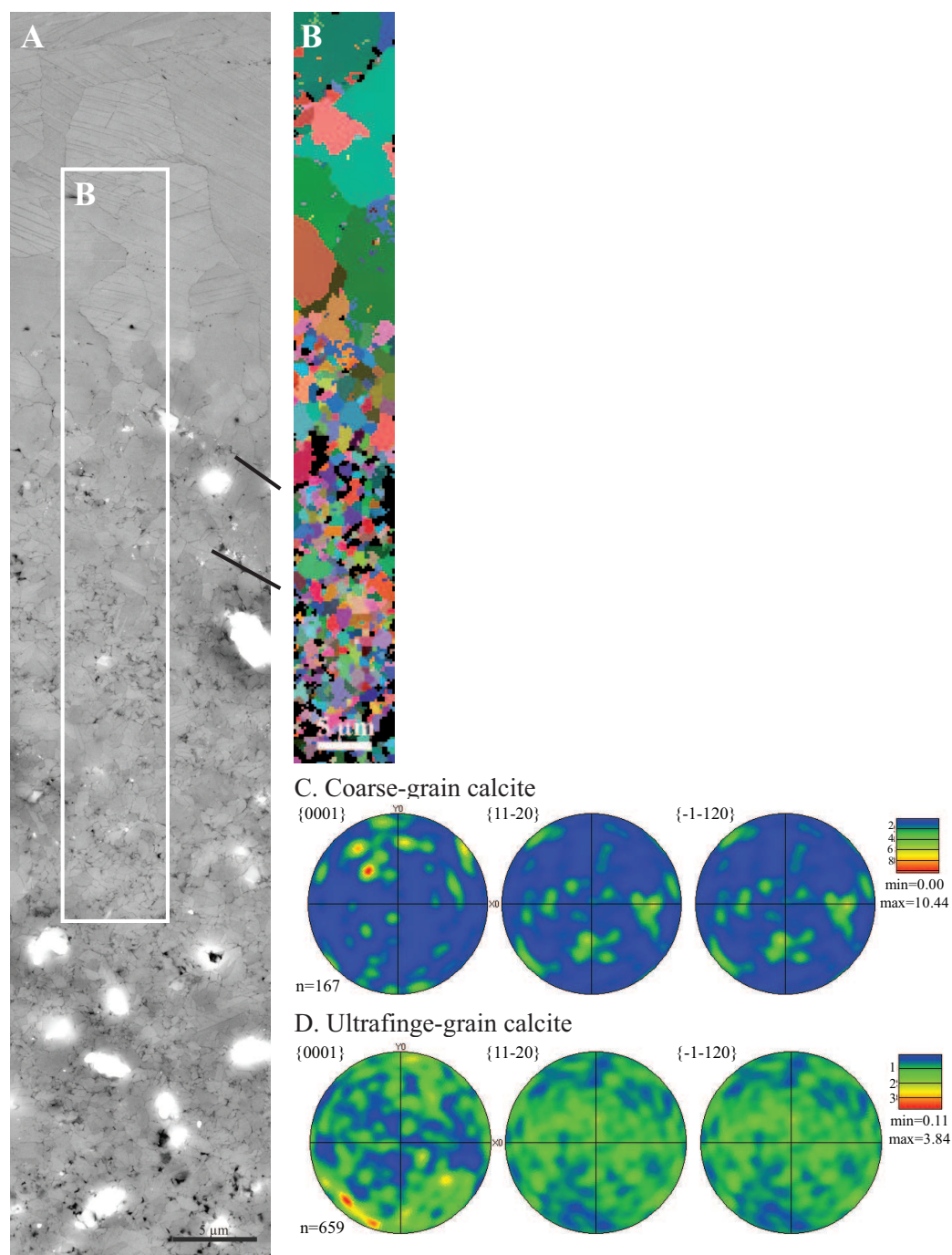


**Figure 8.** EBSD data. (A) Transition from coarse-grained calcite to ultrafine-grained calcite. Aligned grain boundaries (lines). BSE imaging. (B) EBSD map of coarse-grained calcite layer to ultrafine-grained calcite layer. (C) and (D) Contoured plots of one point per grain on the c, a, and r axes on a upper hemisphere projection. Note max contour value differences. (C) Coarse-grained calcite displays a strong maximum, perpendicular to shear zone foliation. (D) No LPO in ultrafine-grained calcite.

#### 4.4 Shear zone

The shear zone is composed of aggregate clasts of ultrafine-grained calcite (5  $\mu\text{m}$  - 400  $\mu\text{m}$ ) and shale (10-350  $\mu\text{m}$ ) surrounded by an interconnected network of ultrafine-grained matrix of mixed calcite and shale (Figure 9a, 9b). The microstructures within the calcite aggregate clasts are similar to the microstructures in the calcite band (section 4.2.3) and in the calcite veins in the shale below (sections 4.2.1 and 4.2.2) (Figure 9b). Within the clasts, areas of coarser-grained ( $>5$   $\mu\text{m}$ ) calcite contain trails of voids along twin boundaries and voids at twin-twin and twin-grain boundary intersections (Figure 7c). Ultrafine-grained ( $<1$   $\mu\text{m}$ ) areas in calcite clasts contain voids at grain boundaries and exhibit interpenetrating grains, and less commonly, fractures and twins (Figure 7c).

Along the edges of the calcite aggregate clasts, individual calcite grains are detached from the clasts (Figure 9c, 9d). Trains of calcite grains are observed adjacent to the clasts, within the mixed shale and calcite matrix (Figure 9c). Calcite matrix grains are finer-grained (mean grain size 0.31  $\mu\text{m}$ ; axial ratio 1:2) (Figure 5d) than matrix shale grains (mean grain size 0.50  $\mu\text{m}$ ), and form an interconnected network around the fine-grained shale matrix grain (Figure 9a; 9b). Calcite-calcite grain boundaries in the shear zone matrix are typically interpenetrating (Figure 9c, 9d). The long axes of calcite grains are dominantly parallel to the shear zone (Figure 5e). While the matrix grain size is only marginally finer than the calcite grain size within the *calcite band*, note that the range of grain sizes is substantially reduced (Figure 5).

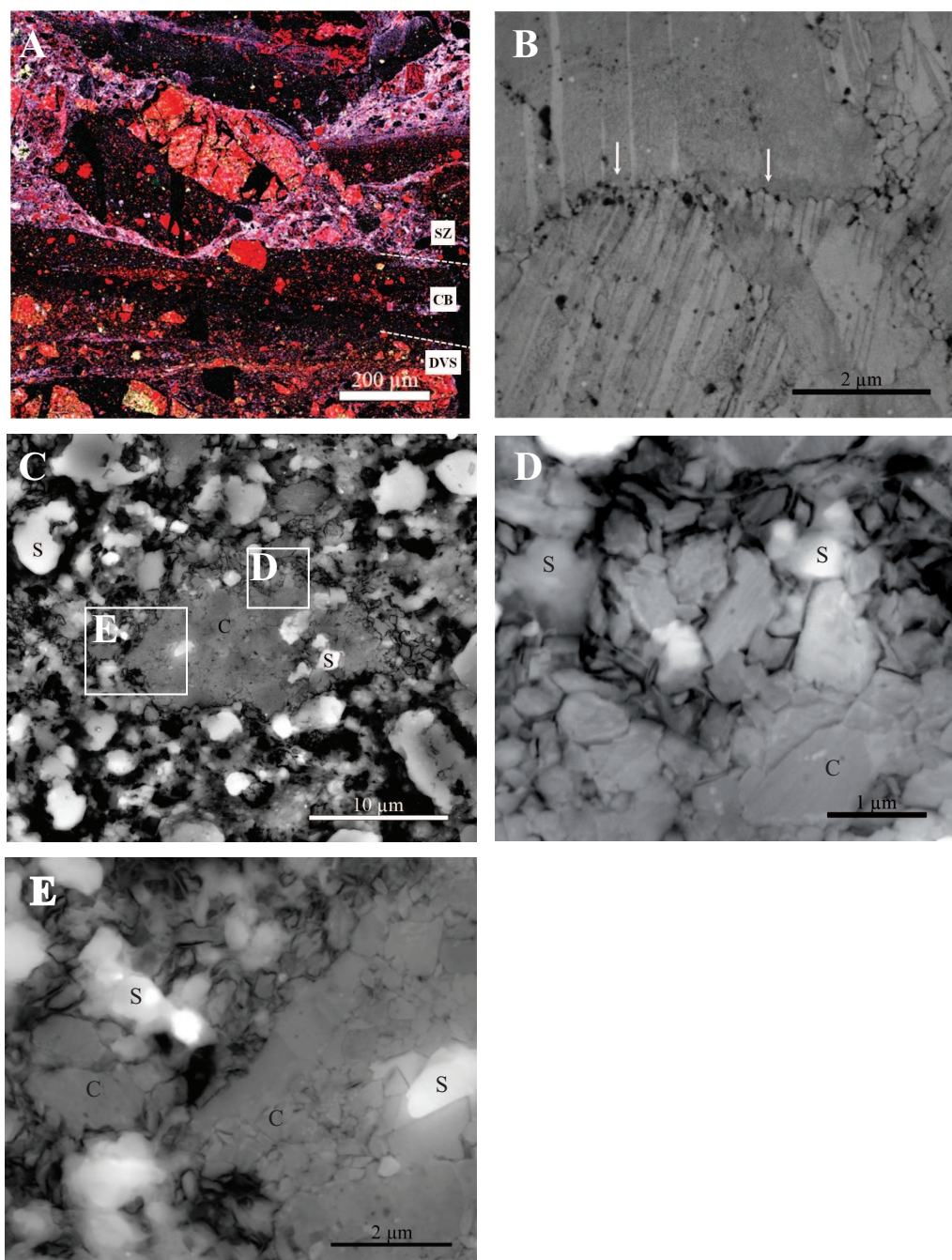


**Figure 9.** Shear zone microstructures. (A) EDS map of the *shear zone* (SZ), *calcite band* (CB), and *densely-veined shale* (DVS). Interconnected network of ultrafine-grained calcite and shale surround calcite aggregate and shale clasts. Si-red, Na-green, K-blue, Al-white, Ca-black. (B) Voids and offset at twin-twin and twin-grain boundary intersections. (C) Calcite aggregate clast surrounded by shale (s) and ultrafine-grained calcite (c). BSE imaging. (C) Detached and interpenetrating grain boundaries at calcite clasts edge. SE imaging. (D) Edge of calcite aggregate clast. BSE imaging.

## 5. DISCUSSION

While the footwall and hanging wall of the CC thrust fault are composed of shale, calcite veins, emplaced parallel to the shear zone at the shear zone-footwall boundary, played the critical role in accommodating displacement along this fault zone. The formation of the fault parallel and perpendicular veins, particularly at the base of the shear zone, was intermittent during the fault zone deformation. The calcite underwent significant grain size reduction to  $<1 \mu\text{m}$ , and the resulting ultrafine-grained calcite deformed by multiple, concurrent deformation mechanisms that contributed to grain boundary sliding. These processes are discussed, below.

### 5.1. Grain size reduction

Grain size reduction from  $>5 \mu\text{m}$  to  $<1 \mu\text{m}$  is observed in calcite veins where fault-parallel veins cross-cut fault-perpendicular veins within the footwall shale, as well as in the fault-parallel *calcite band* at the shear zone-footwall contact. Within coarse calcite grains, voids occur in trails following twin boundaries (Figure 7a), and are especially pronounced at observed twin-twin intersections (Figure 7b). The voids at these intersections suggest that twin boundaries were obstacles to twin boundary glide, resulting in stress concentrations and plasticity (twinning) – induced fracturing (e.g., Mitra, 1978). The unusual square to rectangular shape of the calcite grains (Figure 7c) further suggests that the twins exerted control over the fracturing that formed the ultrafine-grains (Figure 7c). The voids observed at the intersections of twins and grain

boundaries (Figure 7c; 7e) suggest that grain boundary mobility at these intersections was limited, further contributing to grain size reduction.

Intermediate-sized grains ( $\sim 2 \mu\text{m}$ ), observed locally at the boundary between coarse and ultrafine grained layers within the *calcite band*, exhibit curved grain boundaries as well as variable grayscales in BSE images within grains suggesting a contribution to grain size reduction from dislocation accommodated dynamic recrystallization. Variable grayscales in BSE images suggest variations in lattice orientation within the grains that may represent subgrains and suggest subgrain rotation recrystallization. Irregular twin boundaries are observed as well (Figure 7b), resulting in  $\sim 1 - 2 \mu\text{m}$  grains, suggesting a contribution to the reduced grain size from twin boundary migration recrystallization. However, these intermediate size grains ( $\sim 2 \mu\text{m}$ ) are only rarely observed, suggesting that dislocation processes did not contribute significantly to grain size reduction. Note, as well, that the  $\sim 2 \mu\text{m}$  calcite grains that result from these processes are significantly coarser than the  $\sim 0.3 \mu\text{m}$  calcite grains observed in the ultrafine-grained layers of the *calcite band* and in the *shear zone* (Figure 5c, 5d).

## 5.2. Multiple deformation mechanisms

### 5.2.1 Calcite

Microstructures within the coarse ( $>5 \mu\text{m}$ ) layers and fine-grained ( $<1 \mu\text{m}$ ) layers of the calcite band suggest that the layers experienced different deformation histories. Within the coarse-grained layers, twins are common (Figure 7d). The orientations of

grains within a coarse-grained layer indicate a strong LPO developed during deformation with c-axes oriented perpendicular to the shear zone foliation (Figure 8). The strong LPO is evidence for crystal plasticity within the coarse-grained calcite during deformation. The frequent voids at twin-twin and twin-grain boundary intersections observed in coarser grained calcite in clasts in the shear zone suggest plasticity-induced fracturing (Figure 9b; as described in section 5.1), and indicate that dislocation climb was limited in the coarse calcite grains.

Intermediate-size grains ( $\sim 2 \mu\text{m}$ ) that occur locally between coarse and ultrafine layers, as described in section 5.1, suggest that dislocation processes and subgrain rotation recrystallization were active locally.

The ultrafine-grained layers exhibit microstructures similar to the microstructures observed in vein intersections within the shale layers below. These layers exhibit a variety of microstructures, including twins, intragranular fractures, interpenetrating grain boundaries, four-grain junctions, voids at grain boundaries, and, rarely, irregular twin boundaries (Figure 7b, 7c, 7e). Twins within the ultrafine-grained calcite are one of the least common microstructures and are likely remnant from coarser grains, as we have observed no relationship between twins and locations of likely stress concentration (Newman, 1994). Calcite grains with twins are frequently cross-cut by other microstructures, particularly intragranular fractures (Figure 7c, 7e). Interpenetrating grain boundaries are the most common microstructure that we observe (Figure 7c, 7e), and are common between grains that contain twins and/or intragranular fractures, and cross-cut these other microstructures (Figure 7c, 7e). The interpenetrating grain

boundaries suggest grain boundary mobility that could result from either diffusive mass transfer or dislocation-accommodated grain boundary migration. The interpenetrating grain boundaries are, however, frequently angular (Figure 7c, 7e), and the radii of curvature are far smaller than in the 1-2  $\mu\text{m}$  grains observed locally from dynamic recrystallization, suggesting that diffusive mass transfer is more likely (Figure 7d).

Four-grain junctions are common in the ultrafine-grained calcite and suggest grain boundary sliding (Drury and Humphries 1988; Passchier and Trouw, 2005), likely accommodated by diffusive mass transfer at grain boundaries. The lack of a LPO further supports the interpretation that diffusion accommodated grain boundary sliding was the dominant deformation mechanism within the ultrafine-grained calcite layers. Grain boundary alignments continuous across many grains (Figure 7d, Figure 8a) within the ultrafine-grained layers of the *calcite band* suggest that grain boundary sliding along these surfaces also contributed to the deformation. The grain orientation map of the ultrafine-grained calcite (Figure 8b) shows no groupings of grains of similar orientations, indicating that individual ultrafine grains have moved relative to one another, and are not static, fractured remnants of coarser grains. Movement of the calcite grains likely contributed to mixing of shale with the ultrafine-grained calcite (4.5%), as well as the formation of porosity, which increases from 1% in the coarse-grained calcite to 6% in the ultrafine-grained calcite. The voids along grain boundaries, largely parallel to the shear zone (Figure 4c) and veins below in the *shale layer* and *densely-veined shale layer*, suggest that grain growth was not able to keep pace with



strain within the deforming zone.

### 5.2.2 *Shale*

Sedimentary laminations within the shale layer, and observed locally within the densely-veined shale layer, suggest that the shale did not experience penetrative deformation. Rather, shale deformation was dominated by vein-forming brittle fracture. The similarity in orientation of the voids within the deforming calcite band and the veins in the shale, below, suggest that the shale continued to deform by brittle fracture during deformation of the calcite.

### 5.3. *Mixing of ultrafine-grained calcite and shale within shear zone*

The shear zone is composed of calcite aggregate clasts and shale clasts within an interconnected network of ultrafine-grained calcite and shale. The calcite aggregate clasts display microstructures similar to those observed within the ultrafine-grained layers of the *calcite band* (ultrafine-grained, interpenetrating grain boundaries; compare Figure 9c, 9d and Figure 7e, 7f), suggesting that the aggregate calcite clasts originated as vein calcite.

Individual calcite grains along the edges of the calcite aggregate clasts are detached from the clasts and are entrained within the matrix, mixing with shale (Figure 9c, 9d). The mixed ultrafine-grained matrix calcite and shale form an interconnected network around the remaining clasts. Within the matrix, the ultrafine-grained calcite forms an interconnected network around the matrix shale, suggesting that within the



matrix, the ultrafine-grained calcite forms the stress-supporting network, and controls the strength of the shear zone rocks. Interpenetrating grain boundaries suggest that the ultrafine-grained matrix calcite deformed primarily by grain boundary sliding accommodated by diffusion creep. The equation for diffusion creep is

$$\dot{\epsilon} = \frac{A}{d^3} e^{\left(-\frac{H}{RT}\right)} \sigma^1, \quad (1)$$

where  $d$  – grain size,  $T$  – temperature,  $\dot{\epsilon}$  – strain rate, and  $\sigma$  – stress. The ultrafine-grain size of the calcite (0.31  $\mu\text{m}$ ) suggests that the calcite, deforming by grain size sensitive diffusion creep, and therefore the shear zone, was very weak.

#### 5.4. Intermittent vein formation

The coarse and ultrafine-grained layers within the calcite band suggest intermittent vein formation during deformation. The grain boundary alignments observed in the ultrafine-grained calcite layers are cross-cut by the coarse-grained calcite layers (Figure 7d; Figure 8a), indicating that the coarse-grained layers are younger than the ultrafine-grained calcite. The coarse-grained layers likely formed as fractures within the ultrafine-grained calcite layers, within which calcite precipitated. Coarse-grained calcite layers are likely the starting material for the ultrafine-grained calcite.

Additional evidence for intermittent vein formation is found in the comparison of the texture of the coarse-grained calcite and ultrafine-grained calcite in the *calcite band* (Figure 7d, 7f, 7g; Figure 8). Areas of coarse-grained calcite display a maximum of  $c$ -axes oriented perpendicular to the shear zone foliation, while areas of ultrafine-grained

calcite contain no LPO. The newly precipitated calcite more easily deformed by crystal-plastic mechanisms, such as dislocation glide and twinning. As strain increased, twinning was insufficient to accommodate the strain, stress concentrations occurred at twin-twin intersections, resulting in intragranular fractures and a reduction in grain size. The ultrafine grains deformed by grain boundary sliding, thus destroying the LPO in ultrafine-grained layers. As new veins formed, this process was repeated, resulting in layers within the calcite band with different grain sizes, deformed by different deformation mechanisms.

The repeated emplacement of calcite veins within one zone at the contact between the shear zone and the footwall, resulting in a thick calcite band 300  $\mu\text{m}$  thick, further suggests that the ultrafine-grained calcite represented a weak zone. While the intermittent vein formation may have contributed to strain along the CC thrust fault by displacement associated with the formation of the calcite veins, the more significant contribution from these fluids was the precipitation of calcite that served as the starting material for the weak ultrafine-grained calcite that deformed by diffusion accommodated grain boundary sliding (GBS).

#### *5.5. Evolution of fault zone rheology*

The microstructures in the shear zone and footwall of the CC suggest an interpretation for the evolution of the shear zone, and its rheology. Deformation initiated by fracturing of the shale, likely as a result of high fluid pressure, with the precipitation of calcite veins. The fluids, therefore, were the source of calcite along the footwall-shear

zone contact, as described in section 5.4. The coarse-grained calcite (observed at the base of the shear zone) initially deformed by twining and dislocation glide, resulting in a strong LPO (Figure 8c). Voids at twin-twin and twin-grain boundary intersections suggest that dislocation climb was limited, resulting in stress concentrations at these intersections and plasticity-induced fracturing, the primary mechanism for grain size reduction to an ultrafine grain size (0.34  $\mu\text{m}$ ). Interpenetrating grain boundaries, with very small-radius serrations, 4-grain junctions, frequent voids along grain boundaries and the lack of a LPO, suggest that the ultrafine-grained calcite deformed primarily by grain-size sensitive, grain boundary sliding accommodated by diffusion creep. The similarity in orientation of the voids within the calcite and the veins within the shale, below, suggest that shale continued to deform by brittle fracture as the deformation continued within the calcite, perhaps producing shale clasts that mixed with calcite within the shear zone. Coarse-grained layers within the calcite band that cross-cut grain boundary alignments in the *calcite band* indicate that calcite veins continued to form within the calcite, as well.

Shale clasts and clasts of aggregate calcite from the calcite band were entrained into the shear zone, where they continued to be reduced in size. Calcite grains detached from the aggregate calcite clasts and mixed with shale that continued to fracture, resulting in a fine-grained matrix that anastomoses around remaining clasts. Within the fine-grained matrix, calcite is finer-grained than shale matrix grains, and forms an interconnected network around the shale matrix grains, suggesting that the

rheology of the shear zone was controlled by the deformation of the ultrafine-grained calcite by viscous grain boundary sliding.

Other foreland thrusts, the Hunter Valley in the southern Appalachians, (Wojtal, 1986; Wojtal and Mitra, 1986; Kennedy and Logan, 1998) and the McConnell thrust, in the Canadian Rockies (Kennedy and Logan 1997), contain similar lithologies, and have experienced similar displacements at similar conditions as the Copper Creek thrust fault. However, both the Hunter Valley and McConnell thrust faults developed a 1 m thick zone of penetrative deformation (Wojtal and Mitra, 1986; Kennedy and Logan, 1997; 1998), compared to the 2 cm thick zone along the CC thrust, suggesting that the rheology of the CC thrust is weaker than the Hunter Valley and McConnell thrust faults. Fracturing followed by dynamic recrystallization reduced grain size along the Hunter Valley (~3  $\mu\text{m}$  grain size) and McConnell (~1  $\mu\text{m}$  grain size) thrust faults (Wojtal and Mitra, 1986; Kennedy and Logan, 1997; 1998). Along the CC thrust, however, plasticity-induced fracturing dominated within the coarse-grained calcite, reducing grain size to 0.34  $\mu\text{m}$ .

One possible reason for the different behaviors along these faults is that deformation may have occurred at different temperatures. Both the CC and the Hunter Valley thrust faults formed during the same Allegheny Orogeny, and reached temperatures of 100-180  $^{\circ}\text{C}$  (Wojtal and Mitra, 1986), based on reconstructed cross-sections (Harris, 1976; Harris and Milici, 1977), so that variations in temperature may not be easy to explain. Elevated fluid temperatures at Hunter Valley may have contributed to the development of higher temperature deformation mechanisms, such as

dislocation climb. However, Kennedy and Logan (1997) suggested that the McConnell thrust experienced slightly higher temperatures of 200-300 °C, which may have allowed dislocation climb, so that intragranular fractures from dislocation pile-ups did not form. While all three faults formed narrow shear zones, the shear zone at CC is an order of magnitude narrower, as a result of the mechanism for grain size reduction. Plasticity-induced fracturing at CC resulted in an ultrafine-grain size and a different dominant deformation mechanism than resulted from dynamic recrystallization along the other thrusts. The finer grain size at CC, deforming by diffusion accommodated GBS, thus resulted in a weaker rheology and a narrower shear zone.

Another possible reason for the variation in grain size and thickness of the shear zone is differences in lithologies between the three faults. All three faults are carbonate-shale thrust faults (Wojtal and Mitra, 1986; Kennedy and Logan, 1997; 1998); however, the Hunter Valley thrust contains dolomite (clasts and veins) and quartz clasts (Wojtal and Mitra, 1986) and the McConnell thrust also contains dolomite (Kennedy and Logan, 1997). The CC thrust only contains calcite and shale. The different strengths of calcite (Rutter, 1995; Brodie and Rutter, 2000a) and dolomite (Davis et al., 2008; Delle Piane et al., 2008) and quartz (Griggs, 1967; Brodie and Rutter, 2000b) under similar conditions could explain the different behaviors along these faults. The addition of dolomite and quartz within the Hunter Valley and McConnell thrusts, may have contributed to the strength of these shear zones, relative to the CC thrust.

## 6. CONCLUSIONS

The intermittent vein formation along the CC thrust fault contributed to the large displacement along a narrow shear zone primarily by providing the starting material for the weak ultrafine-grained calcite that deformed by diffusion accommodated GBS. The microstructures in a transect from the footwall to the shear zone along the CC thrust fault suggest the following evolution of rheology:

1. Areas of coarse- and ultrafine-grained calcite near the shear zone-footwall contact are the result of intermittent vein formation.
2. Stress concentrations at twin-twin and twin-grain boundary intersections in coarse-grained calcite resulted in intragranular fractures. This plasticity-induced fracturing reduced the grain size within the calcite grains to  $<1.0 \mu\text{m}$ .
3. Within coarse-grained calcite, the dominant deformation was by plasticity-induced fracturing. Once grain size was reduced, ultrafine-grained calcite grains deformed by brittle, diffusive, and plastic deformation mechanisms.
4. Shale deformation, concurrent with calcite deformation, was dominated by brittle fracture.

5. Formation of an interconnected network of the ultrafine-grained calcite, in the *shear zone*, suggests calcite, not the shale, was the weak phase. The resulting ultrafine-grained calcite flowed by diffusion creep accommodated GBS, leading to a weak interconnected network around the shale that enabled large displacement along the narrow shear zone.

.

## REFERENCES

- Brodie, K.H., Rutter, E.H., 2000a. Deformation mechanisms and rheology: why marble is weaker than quartzite. *Journal of Geological Society* 157, 1093-1096.
- Brodie, K.H., Rutter, E.H., 2000b. Rapid stress release caused by polymorphic transformation during the experimental deformation of quartz. *Geophysical Research Letters* 27, 3089-3092.
- Cobbold, P.R., Clarke, B.J., Løseth, H., 2009. Structural consequences of fluid overpressure and seepage forces in the outer thrust belt of the Niger Delta. *Petroleum Geoscience* 15, 3-15.
- Dahlen, F.A., 1990. Critical taper model of fold-and-thrust belts and accretionary wedge. *Annual Review Earth Planet Science* 18, 55-99.
- Dahlen, F.A., Suppe, J., Davis, D., 1984. Mechanics of fold-and-thrust belts and accretionary wedge: cohesive coulomb theory. *Journal of Geophysical Research* 89, 10,087-10,101.
- Davis, D.M., Engelder, T., 1985. The role of salt in fold-and-thrust belts. *Tectonophysics* 119, 67-88.
- Davis, N.E., Kronenberg, A.K., Newman, J., 2008. Plasticity and diffusion creep of dolomite. *Tectonophysics* 456, 127-146.
- Delle Piane, C., Burlini, L., Kunze, K., Brack, P., Burg, J.P., 2008. Rheology of dolomite: large strain torsion experiments and natural examples. *Journal of Structural Geology* 30, 767-776.
- Drury, M.R., Humphries, F.J., 1988. Microstructural shear criteria with grain-boundary sliding during ductile deformation. *Journal of Structural Geology* 10, 83-89.
- Griggs, D., 1967. Hydrolytic weakening of quartz and other silicates. *The Geophysical Journal of the Royal Astronomical Society* 14, 19-31.



- Harris, L. D., 1976. Thin-skinned tectonics and potential hydrocarbon traps illustrated by a seismic profile in the Valley and Ridge Province of Tennessee. *Journal Research U.S. Geological Survey* 4, 379-386.
- Harris, L. D., Milici, R. C., 1977. Characteristics of thin-skinned style of deformation in the southern Appalachians and potential hydrocarbon traps. U.S. Geological Survey Professional Paper 1018, 1-40.
- Hubbert, M.K., Rubey, W.W., 1959. Role of fluid pressure in mechanics of overthrust faulting, I: mechanics of fluid-filled porous solids and its application to overthrust faulting. *Geological Society of America Bulletin* 70, 115-166.
- Ikari, M.J., Saffer, D.M., Marone, C., 2009. Frictional and hydrologic properties of clay-rich fault gouge. *Journal of Geophysical Research* 114, 1-18.
- Kennedy, L.A., Logan, J.M., 1997. The role of veining and dissolution in the evolution of fine-grained mylonites: the McConnell thrust, Alberta. *Journal of Structural Geology* 19, 785-797.
- Kennedy, L.A., Logan, J.M., 1998. Microstructures of cataclasites in a limestone-on-shale thrust fault. *Tectonophysics* 295, 167-186.
- Lemiszi, P.J., Kohl, M.S., 2006. Geologic excursion across part of the Southern Appalachian foreland fold-thrust belt in northeastern Tennessee. Southeastern Section meeting, Geological Society of America, 37-64.
- Liu, J., Walter, J.M., Weber, K., 2002. Fluid-enhanced low-temperature plasticity of calcite marble: microstructures and mechanisms. *Geology* 30, 787-700.
- Mitra, G., 1978. Ductile deformation zones and mylonites: the mechanical processes involved in the deformation of crystalline basement rock. *American Journal of Science* 278, 1057-1084.
- Mitra, G., 1984. Brittle to ductile transition due to large strains along the White Rock thrust, Wind River mountains, Wyoming. *Journal of Structural Geology* 6, 51-61.

- Newman, J., 1994. The influence of grain size and grain size distribution on methods for estimating paleostresses from twinning in carbonates. *Journal of Structural Geology* 16, 1589-1601.
- Newman, J., Mitra, G., 1993. Lateral variations in mylonite zone thickness as influenced by fluid-rock interactions, Linville Falls thrust, North Carolina. *Journal of Structural Geology* 15, 849-863.
- Newman, J., Mitra, G., 1994. Fluid-influenced deformation and recrystallization of dolomite at low temperatures along a natural fault zone, Mountain City window, Tennessee. *Geological Society of America Bulletin* 106, 1267-1280.
- O'Hara, K., 1988. Fluid flow and volume loss during mylonitization: an origin for phyllonite in an overthrust setting, North Carolina, U.S.A. *Tectonophysics* 156, 21-36.
- O'Hara, K., 1990. State of strain in mylonites from the western Blue Ridge province, southern Appalachians: the role of volume loss. *Journal of Structural Geology* 12, 419-430.
- Passchier, C.W., Trouw, R.A.J., 2005. *Microtectonics*. Springer-Verlag, Berlin, Germany.
- Rutter, E., 1995. Experimental study of the influence of stress, temperature, and strain on the dynamic recrystallization of Carrara marble. *Journal of Geophysical Research* 100, 24,651-24,663.
- Suppe, J., 1985. *Principles of structural geology*. Prentice-Hall Inc, Englewood Cliffs, New Jersey, 285.
- Thomas, T., 2001. Mushwad: ductile duplex in the Appalachian thrust belt in Alabama. *AAPG Bulletin* 85, 1847-1869.
- Wiltschko, D.V., Chapple, W.M., 1977. Flow of weak rocks in Appalachian Plateau folds. *AAPG Bulletin* 61, 653-670.

Wojtal, S., 1986. Deformation within foreland thrust sheets by populations of minor faults. *Journal of Structural Geology* 8, 341-360.

Wojtal, S., Mitra, G., 1986. Strain hardening and strain softening in fault zone from foreland thrust. *Geological Society of America Bulletin* 97, 674-687.

**VITA**

Name: Rachel Kristen Wells

Address: Department of Geology and Geophysics, MS 3115, College Station,  
TX, 77843

Email Address: wellsrk@gmail.com

Education: B.S., Geology, The University of Texas at Austin, 2006  
M.S., Geology and Geophysics, Texas A&M University, 2010